



Ultrahigh-energy Cosmic-Ray Interactions as the Origin of Very High-energy γ -Rays from BL Lacertae Objects

Saikat Das^{1,3}, Nayantara Gupta¹, and Soebur Razzaque²¹ Astronomy & Astrophysics Group, Raman Research Institute, Bengaluru 560080, Karnataka, India; saikatdas@rri.res.in, nayan@rri.res.in² Centre for Astro-Particle Physics (CAPP) and Department of Physics, University of Johannesburg, P.O. Box 524, Auckland Park 2006, South Africa
srazzaque@uj.ac.za

Received 2019 November 15; revised 2019 December 10; accepted 2019 December 10; published 2020 February 3

Abstract

We explain the observed multiwavelength photon spectrum of a number of BL Lacertae (BL Lac) objects detected at very high energy (VHE, $E \gtrsim 30$ GeV), using a lepto-hadronic emission model. The one-zone leptonic emission is employed to fit the synchrotron peak. Subsequently, the SSC spectrum is calculated, such that it extends up to the highest energy possible for the jet parameters considered. The data points beyond this energy, and also in the entire VHE range are well explained using a hadronic emission model. The ultrahigh-energy cosmic rays (UHECRs, $E \gtrsim 0.1$ EeV) escaping from the source interact with the extragalactic background light (EBL) during propagation over cosmological distances to initiate electromagnetic cascade down to ~ 1 GeV energies. The resulting photon spectrum peaks at ~ 1 TeV energies. We consider a random turbulent extragalactic magnetic field (EGMF) with a Kolmogorov power spectrum to find the survival rate of UHECRs within 0.1 of the direction of propagation in which the observer is situated. We restrict ourselves to an rms value of EGMF, $B_{\text{rms}} \sim 10^{-5}$ nG, for a significant contribution to the photon spectral energy distribution from UHECR interactions. We found that UHECR interactions on the EBL and secondary cascade emission can fit gamma-ray data from the BL Lac objects we considered at the highest energies. The required luminosity in UHECRs and corresponding jet power are below the Eddington luminosities of the supermassive black holes in these BL Lac objects.

Unified Astronomy Thesaurus concepts: High-energy astrophysics (739); Blazars (164); Relativistic jets (1390); Gamma-rays (637); Ultra-high-energy-cosmic radiation (1733); Extragalactic magnetic fields (507)

1. Introduction

The far-reaching progress made in γ -ray observations in the last decade and the considerable amount of data collected by *Fermi*-LAT (Ackermann et al. 2015; *Fermi*-LAT Collaboration et al. 2015), MAGIC (Acciari et al. 2019), HESS (Aharonian et al. 2006), VERITAS (VERITAS Collaboration et al. 2018), and HAWC (Abeysekara et al. 2017a, 2017b) experiments, etc., have evolved the understanding of our universe in the high-energy (HE) regime. The precision measurement of photon fluxes from a wide variety of astrophysical objects provides an impetus to study the γ -ray sky as a probe of various hadronic interaction processes. It also tests speculations on the origin of ultrahigh-energy cosmic rays (UHECRs), i.e., particles with energies beyond 10^{18} eV and extending up to a few times 10^{20} eV.

Active galactic nuclei (AGNs) are a class of astrophysical objects that are considered to be the potential acceleration sites of UHECRs. The collimated beam of outflow from an AGN contains a tangled magnetic field and a relativistic population of electrons and protons, assumed to be accelerated by the same physical process. These jets transport energy and momentum over large distances by hosting a variety of interactions and radiative emission processes, thus injecting high-energy particles into the universe. A particular subclass of radio-loud AGNs called blazars have their relativistic jets oriented closely along the line of sight of the observer. The non-thermal continuum emission from blazars span over a wide range of frequencies, from radio to very high-energy (VHE) γ -rays ($E > 30$ GeV), and exhibit variability at diverse timescales, which may or may not be coherent in all wavebands. The spectral energy distribution (SED) of blazars

show two distinct components—a low-energy peak between optical and X-ray energies and a high-energy peak in the γ -ray regime. While the former is attributed to synchrotron emission of relativistic electrons accelerated in the jet, several propositions exist for the latter. The most prevalent explanation in light of the leptonic model invokes the inverse-Compton (IC) scattering of synchrotron photons (SSC) or external photons (accretion disk, dusty torus, or broad-line region) by the same population of relativistic electrons. This allows the detection of VHE γ -rays due to relativistic beaming of the emitted photons from the jet. Alternately, hadronic models predict that high-energy protons inside the jet can produce electron-positron pairs (e^+e^-) and charged/neutral pions (π^0, π^\pm) by photohadronic interactions. The e^+e^- pairs can undergo synchrotron emission losses and the neutral pions decay to produce γ photons. The charged pions and muons produced in these photohadronic interactions can also radiate by synchrotron process before decaying into electrons. The mass of pions and muons being two orders of magnitude higher than electrons, the efficiency of such loss is lower than electron synchrotron radiation in general. Also possible is the proton synchrotron emission peaking at multi-TeV energies (Aharonian 2002). However, the latter requires very high jet power, which may surpass the Eddington luminosity (L_{Edd}) in some cases (Zdziarski & Böttcher 2015). Interpreting the multiwavelength spectrum using lepto-hadronic models requires a minimum jet power, which is crucial to understanding the interactions and physical properties inside the jet (Böttcher et al. 2013).

High-frequency peaked BL Lacertae (BL Lac) objects (HBLs) have their peak synchrotron emission in the UV-to-X-ray energy range and their spectrum extends up to multi-TeV energies. They comprise the majority of extragalactic VHE γ -ray sources. At these extreme energies, the high-energy

³ Corresponding author.

photons if produced inside the jet can be absorbed by intrinsic $\gamma\gamma$ pair production with target photons originating from the broad-line region (BLR), dusty torus (DT), or accretion disk. They will also suffer attenuation losses due to γ_{bg} collision with the extragalactic background light (EBL) photons while propagating over cosmological distances, hence the intrinsic spectrum must be harder than the observed spectrum. For some HBLs, the intrinsic spectrum at TeV energies is too hard to be explained by the one-zone leptonic model due to suppression of IC emission through the Klein-Nishina (KN) effect and intrinsic/extrinsic pair production losses. The TeV spectra can be explained by another scenario, in which the UHECRs from the sources interact with the cosmic background photons to produce electromagnetic (EM) particles, viz., electrons, positrons, photons (see Essey & Kusenko 2010). These secondary particles can initiate electromagnetic cascade and produce a resultant γ -ray spectra at VHE range (Essey et al. 2010, 2011b; Murase et al. 2012; Razzaque et al. 2012; Kalashev et al. 2013; Supanitsky & de Souza 2013; Takami et al. 2013; Tavecchio 2014; Khalikov & Dzhatdov 2019). Such a scenario is applicable for HBLs at redshifts greater than the mean interaction length of UHECR protons for photohadronic interactions, and lesser than the distance where a majority of the photons produced are either scattered off from the line of sight or absorbed completely by the EBL photons. These cascade photons can contribute significantly to the spectrum at the highest observed energies. Resonant photopion production in the cosmic microwave background (CMB) occurs for protons with energies $E \geq 50$ EeV. At lower energies, interactions with the EBL photon dominates.

In this paper, we consider a representative sample of HE BL Lac objects, for which the TeV emission is prominent and non-variable, and the source parameters are suitable for UHECR acceleration. More than 3130 of the identified or associated sources in the 50 MeV–1 TeV range, listed in the *Fermi*-LAT 8 yr source catalog (4FGL), are blazars (The *Fermi*-LAT Collaboration 2019a). The 4LAC catalog, which is the companion of 4FGL focused on AGNs, splits the blazar candidates based on their spectral properties into 650 flat-spectrum radio quasars (FSRQs) and 1052 BL Lac objects with 1092 blazars of unknown type (The *Fermi*-LAT Collaboration 2019b). While a majority of FSRQs are low-synchrotron peaked, the BL Lac objects are fairly evenly distributed between low-synchrotron peaked, intermediate-synchrotron peaked, and high-synchrotron peaked subclasses. The redshift is unknown for the majority of BL Lac objects. However, the redshifts of the sources considered in this work are well studied. We model the multiwavelength SED in the quiescent state by a one-zone leptonic synchrotron/SSC model that extends up to the highest energies allowed by the leptonic model. Next, we fit the data points in the VHE range by secondary photons originating from UHECR interactions while propagating in the CMB and EBL close to the line of sight. The requirement of this additional component is compelling for the SED of HBLs considered in this analysis. During the propagation of UHECR protons, they are subjected to deflections by the EGMF. The EGMF is not known to high precision. We set constraints on the rms value of the EGMF, such that a significant fraction of UHECR protons are constricted near to the line of sight, respecting the luminosity budget. We calculate the required kinetic power in electrons and protons to compare it with the Eddington luminosity of the AGN.

The hindrance due to EGMF, in addition to the EBL attenuation of photon fluxes originating from the jet increases the required total jet power to explain the SED. The plausibility of hadronic interactions inside the jet has been studied earlier

in great details (Sahu et al. 2012; Böttcher et al. 2013; Petropoulou & Mastichiadis 2015; Sahu et al. 2019; Xue et al. 2019b). However, the efficiency of photon production in such a scenario can be correlated directly with the internal pair production, owing to the same seed photon distribution in both processes (Böttcher & Els 2016). The interaction efficiency of photohadronic interactions in the high-energy limit is 10^{-3} times smaller than the peak $\gamma\gamma$ opacity, leading to a substantial reduction in the escaping photon flux (Murase et al. 2018). In our model, we calculate the opacity of $p\gamma$ interactions inside the jet to find that the contribution from such interactions is insignificant and escape by diffusion dominates for protons up to ultrahigh energies.

Also, if neutrinos are produced in the same UHECR interactions as photons, they must contribute to the observed neutrino flux at the highest energies. The upper limits to the neutrino flux come from measurements in the IceCube (Aartsen et al. 2018) and Pierre Auger (Aab et al. 2015) experiments. We find an estimate for the neutrino flux from these high-energy TeV blazars and show that a detection is difficult in the near future owing to the extremely low flux value compared to the current and upcoming detector sensitivities. We discuss the theoretical framework and the model used for the relativistic jet and UHECR propagation in Section 2. We show our results from modeling the multiwavelength SEDs of HBLs and the resultant UHECR and neutrino event rates in Section 3. We discuss the results obtained from our analysis in Section 4 and draw our conclusions in Section 5.

2. Theoretical Framework

2.1. Leptonic Modeling

We consider the emission region inside the jet to consist of a relativistic plasma of electrons and protons moving through a uniform magnetic field B in a spherical blob of radius R . We use a one-zone leptonic model to fit the observed broadband SED and consider the constant spectrum of electrons injected into the system in the comoving frame of the jet as

$$Q_e(E_e) = A_e \left(\frac{E_e}{E_0} \right)^{-\alpha} \exp \left(- \frac{E_e}{E_{e,\text{cut}}} \right) \quad (1)$$

where $E_0 = 0.5$ GeV is a reference energy. The cutoff energy ($E_{e,\text{cut}}$), the injection spectral index (α), and the minimum electron energy ($E_{e,\text{min}}$) are found from modeling the synchrotron spectrum. The resulting IC spectrum is then adjusted to find the highest energy up to which it can extend. Increasing $E_{e,\text{cut}}$ beyond this value may worsen the synchrotron fit or turns out to be ineffective because of KN effect. Electrons and positrons are cooled radiatively by energy loss via synchrotron emission and synchrotron self Compton (SSC) emission processes. We use the open-source code GAMERA⁴ to model the SED up to the highest energies possible using the leptonic model. It solves the one-dimensional (1D) transport equation,

$$\frac{\partial N_e}{\partial t} = Q_e(E_e, t) - \frac{\partial}{\partial E} (bN_e) - \frac{N_e}{t_{\text{esc}}^e} \quad (2)$$

⁴ http://libgamera.github.io/GAMERA/docs/main_page.html

to calculate the spectrum of particles $N_e(E_e, t)$ at a time t , where $b = b(E_e, t)$ is the energy-loss rate of leptons and t_{esc}^e is the timescale on which the leptons escape from the system.

We assume that the electrons escape over dynamical timescale, $t_{\text{esc}}^e = t_{\text{dyn}} = R/c$, which is constant in energy and time. Since the cooling rate for electrons is significantly higher than protons due to radiative losses inside the blob, the escape timescale will be higher and maybe assumed in a simplistic approach to be equivalent to the dynamical timescale R/c . Thus, invoking diffusion loss is not important. For a continuous lepton injection $Q_e(E_e)$, we calculate the resultant spectrum of photons from $N_e(E_e, t)$ at a time much greater than that required to attain the steady state. This ensures that the obtained luminosities are that of the quiescent state and the variabilities, if any, are averaged out.

The photons from the jet are Doppler boosted due to relativistic beaming by a factor of $\delta_D = [\Gamma(1 - \beta \cos \theta)]^{-1}$. Γ is the bulk Lorentz factor, and βc is the velocity of the emitting plasma. $\theta \lesssim 1/\Gamma$ is the viewing angle of the blazar with respect to the line of sight. The synchrotron and SSC luminosities are Doppler boosted by δ_D^4 in the observer frame (Celotti & Ghisellini 2008). The luminosity in electrons required in the AGN frame is given as

$$L_e = \pi R^2 \Gamma^2 c u_e' \quad (3)$$

where $u_e' = (1/V) \times \int_{E_{e,\text{min}}}^{E_{e,\text{max}}} dE_e Q(E_e) E_e$ is the energy density of electrons in the comoving frame of the jet and V is the volume of the blob. The luminosity in magnetic field, i.e., the power carried as Poynting flux is given by

$$L_B = \frac{1}{8} R^2 \Gamma^2 \beta c B^2. \quad (4)$$

It may be possible to explain the entire SED by employing multiple emission zones, and/or other processes involving the geometry of the HBLs. Nonetheless, we restrict ourselves to a single-zone leptonic model only, to accommodate the hadronic component originating from UHECR interactions.

2.2. Hadronic Modeling

Protons are accelerated inside the jet up to maximum energies, which can be estimated from the Hillas condition (Hillas 1984),

$$E_{p,\text{max}} \sim 2\beta c Z e B R. \quad (5)$$

Protons, being heavier than the electrons, are not cooled sufficiently inside the jet and one can simply write $N_p(E_p) = t_{\text{dyn}} Q_p(E_p)$. We find that escape dominates over energy losses inside the jet up to ultrahigh energies. We assume that protons are injected into the ISM following a power-law injection of the form,

$$N_p(E_p) = \frac{dN}{dE_p} = A_p E_p^{-\alpha} \quad (6)$$

where we take $E_{p,\text{min}} = 0.1 \text{ EeV}$ and $E_{p,\text{max}} = 10 \text{ EeV}$. The choice of $E_{p,\text{max}}$ is explained later (see Section 3). We assume the same spectral index for the injection of leptons and hadrons, implying the same inherent acceleration process for both.

For the sake of simplicity, we consider protons ($Z = 1$) as the only UHECRs for this study, and a steep cutoff instead of an exponential one. The signatures of an exponential term is greatly obscured in the resulting photon spectrum, by virtue of

electromagnetic cascade which is primarily driven by CMB and/or EBL photon density, and EGMF. The resonant photopion production of UHECRs with the CMB occurs at $E_p = 50 \text{ EeV}$. In our study, owing to a lower value of $E_{p,\text{max}}$, the dominant contribution to pion decay photons comes from UHECR interactions on the EBL.

The timescales of photohadronic interactions on synchrotron and SSC photons inside the jet are given by

$$\frac{1}{t_{p\gamma}} = \frac{c}{2\gamma_p^2} \int_{\epsilon_{\text{th}}/2\gamma_p}^{\infty} d\epsilon'_\gamma \frac{n(\epsilon'_\gamma)}{\epsilon'^2_\gamma} \int_{\epsilon_{\text{th}}}^{2\epsilon\gamma_p} d\epsilon_r \sigma(\epsilon_r) K(\epsilon_r) \quad (7)$$

where $\sigma(\epsilon_r)$ and $K(\epsilon_r)$ are the cross-section and inelasticity, respectively, of photopion production or Bethe–Heitler pair production as a function of photon energy ϵ_r in the proton rest frame (Stecker 1968; Berezhinskii & Grigor'eva 1988; Chodorowski et al. 1992; Mücke et al. 2000; Berezhinsky et al. 2006). $n(\epsilon'_\gamma)$ is the seed photon density per unit energy interval as a function of photon energy ϵ'_γ in the comoving jet frame. It is related to the observed photon spectrum by the relation (Ghisellini et al. 1993; Joshi & Gupta 2013),

$$4\pi R^2 c \epsilon'^2_\gamma n(\epsilon'_\gamma) = 4\pi d_L^2 \delta_D^{-p} \left(\epsilon'^2_\gamma \frac{dN_\gamma}{d\epsilon_\gamma dt dA} \right)_{\text{obs}} \quad (8)$$

where $p = n + 2$ and $n = 2, 3$ for continuous jet and a moving sphere, respectively. The subscript ‘‘obs’’ in Equation (8) represents the quantity in the observer frame. The photon energy transforms as $\epsilon_r = \delta_D \epsilon'_\gamma / (1 + z)$. For a source at redshift z from the observer, $d_L = (1 + z)d_c$ is the luminosity distance and d_c is the comoving distance. The escape timescale of protons from the source is given as

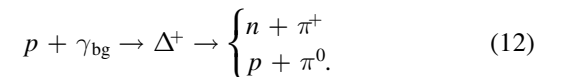
$$t_{\text{esc}}^p = \frac{R^2}{4D} \quad (9)$$

where we write the diffusion coefficient as $D = D_0 (E/E_0)^{2-q}$, where q is the turbulence spectral index and is taken to be $q = 3/2$ for the Kraichnan model. The acceleration timescale is calculated from

$$t_{\text{acc}}^p \simeq \frac{20\eta r_L}{3 c} \simeq \frac{20\eta \gamma_p m_p c}{3 e B}. \quad (10)$$

η is the ratio of the mean magnetic field energy density to the turbulent magnetic field energy density (Lagage & Cesarsky 1983). We consider $\eta = 1$ in our calculations.

The escaping protons propagate through extragalactic distances interacting with the CMB and EBL, producing electrons, positrons, γ -rays, and neutrinos through Δ -resonance or Bethe–Heitler pair production, given as



The neutral pions decay to produce γ photons ($\pi^0 \rightarrow \gamma\gamma$) and the charged pions decay to produce neutrinos ($\pi^\pm \rightarrow \mu^\pm + \nu_\mu \rightarrow e^\pm + \nu_e + \bar{\nu}_\mu + \nu_\mu$). The secondary photons and electrons can initiate electromagnetic cascades down to GeV energies. The secondary γ photons interact with cosmic background radiations and universal radio background (URB), leading to Breit–Wheeler pair production or double

pair production. The relativistic cascade electrons and positrons also lose energy by synchrotron radiation on deflections in EGMF, triplet pair production, and IC scattering of background photons. The neutrinos, on the other hand, once produced propagate rectilinearly unhindered by EGMF or interactions. The proton luminosity required in the AGN frame is calculated as

$$L_p = \pi R^2 \Gamma^2 c u'_p, \quad (13)$$

We use the public astrophysical simulation framework CRPROPA 3 to propagate the UHECR protons from the source to observer (Alves Batista et al. 2016). CRPROPA 3 provides two external codes, DINT (Lee 1998) and EleCa (Settimo & De Domenico 2015), to calculate the development of EM cascades. DINT solves the transport equations to produce the observed spectrum and is thus computationally more efficient. EleCa, on the other hand, does a full Monte Carlo tracking of individual particles. For 1D simulations, DINT can also be combined with EleCa or CRPROPA (Heiter et al. 2018). We propagate the EM particles produced from UHECR interactions using DINT only. We consider the Gilmore et al. EBL model (Gilmore et al. 2012) and a random turbulent EGMF with a Kolmogorov power spectrum of rms field strength $B_{\text{rms}} = 10^{-5}$ nG.

The total luminosity of the HBL is obtained as $L_{\text{jet}} = L_e + L_p + L_B$. We compare the obtained value of L_{jet} with the Eddington luminosity L_{Edd} of the supermassive black hole (SMBH). Thus, we can check whether a scenario that invokes UHECR interactions can account for the origin of γ -rays observed at the highest energies from the HBLs.

3. Results

We explore the effect of our choice of the extragalactic magnetic field (EGMF). The root mean square deflection in the trajectories of cosmic rays on propagation over a distance D in a random turbulent magnetic field with coherence length l_c can be approximated as (Dermer et al. 2009),

$$\Phi_{\text{rms}} \approx 4^\circ \frac{60 \text{ EeV}}{E/Z} \frac{B_{\text{rms}}}{10^{-9} \text{ G}} \sqrt{\frac{D}{100 \text{ Mpc}}} \sqrt{\frac{l_c}{1 \text{ Mpc}}}. \quad (14)$$

The constraints on turbulent EGMF models derived from the correlation between observed UHECR arrival directions and potential AGN sources yield the condition $B_{\text{rms}} \sqrt{l_c} \leq 10^{-9} \text{ G} \sqrt{\text{Mpc}}$ (Pierre Auger Collaboration et al. 2008). One finds from Equation (14), the deflection of a proton of 1 EeV traversing a distance of 1 Gpc from the source to the observer through an EGMF with $B_{\text{rms}} = 10^{-5}$ nG to be $\approx 0^\circ.0076$. In realistic scenarios, the emitted UHECRs are not monoenergetic, but follow a distribution according to Equation (6). We run three-dimensional (3D) test simulations in CRPROPA 3 for the propagation of UHECRs from a source at a distance 1000 Mpc away from the observer to check the effect of varying B_{rms} . We consider a magnetic field with Fourier modes taken from a Gaussian distribution with $\langle |B(\mathbf{k})|^2 \rangle$ given by a Kolmogorov power spectrum and random polarization. In all cases, we set the value of the turbulent correlation length $l_c = 1$ Mpc and thus take the observer to be a sphere of radius $R_{\text{obs}} = 1$ Mpc. The proton injection spectrum is assumed to be a power law, $dN/dE_p \propto E^{-\alpha}$ with $\alpha = 2$ and energies in the range 0.1–10 EeV. All energy-loss processes, viz., photopion production, Bethe–Heitler interaction, nuclear decay and adiabatic expansion of the universe are accounted for in the simulation. The emission from the source is such that almost all of the

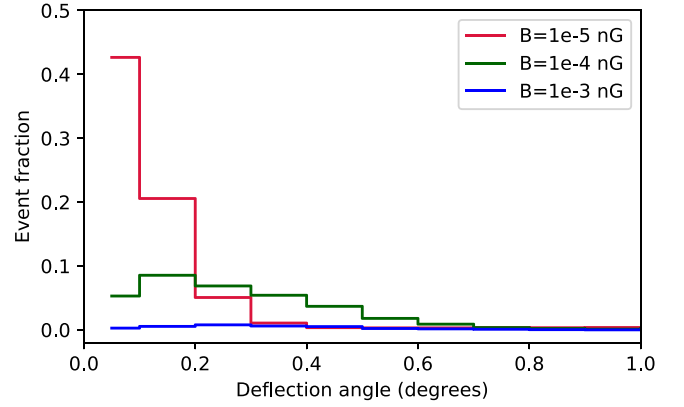


Figure 1. Distribution of propagated UHECRs as a function of deflection angle in a random turbulent magnetic field.

emitted protons are initially directed toward the observer. The deflections of the UHECRs on arrival at the surface of the observer sphere are calculated from initial and final momentum vector directions, and the distribution of observed events as a function of deflection angle is shown in Figure 1. Here the events are binned over deflection angle with respect to the direction along which the UHECRs are emitted, in bin widths of $0^\circ.1$. The event fraction within 0° – $0^\circ.1$ indicates the survival rate of UHECRs close to the initial direction of propagation.

The survival rate of UHECRs increases with decreasing B_{rms} , as well as with higher containment angles. Since we are interested in the calculation of contribution from UHECR interactions to the observed γ -ray SEDs of HBLs, we find the survival rate of UHECRs within $0^\circ.1$ of the direction of propagation in which the observer is positioned and denote it by ξ_B . Accordingly, from the results of the 3D simulations, we consider $B_{\text{rms}} = 10^{-5}$ nG for the rest of our study, to increase the fraction of events close to the direction of jet emission axis of HBLs. In some studies, a lower bound of $\sim 10^{-6}$ nG is found for the EGMF (Neronov & Vovk 2010), while others have estimated it to be as low as 10^{-7} nG (Razzaque et al. 2012) or 10^{-8} nG (Essey et al. 2011a). An increase in the survival rate along the direction of emission for blazars will essentially increase the detection rate along the line of sight of the observer. The angular resolution of *Fermi*-LAT for observation of a single photon at $E > 10$ GeV is $\sim 0^\circ.15$ (The *Fermi*-LAT Collaboration 2019a).

Figure 2 shows the jet emission axis by a vertical solid line directed upwards. The sphere has a radius d_L equivalent to the luminosity distance from the source to the observer. The source is at the center of the sphere. The cone is the extrapolation of the jet emission from the HBL, with a semi-apex angle equal to the jet opening angle θ_{jet} . The observer is at the position where the dashed line pierces through the surface of the sphere. The line of sight is thus directed toward the center of the sphere along the line passing through the observer, and may also lie outside the emission cone. When the line of sight lies outside the jet opening angle, the collimation of outflow along the observer’s direction becomes poor and thus the required jet power increases. However, we do not include any angular dependence for varying observer position in our analysis and assume the jet emission stays collimated along the line of sight. The observer sphere is not shown in this diagram since $R_{\text{obs}} \ll d_L$. Assuming the angle between the emission direction and line of sight to be a few degrees, the viewing angle

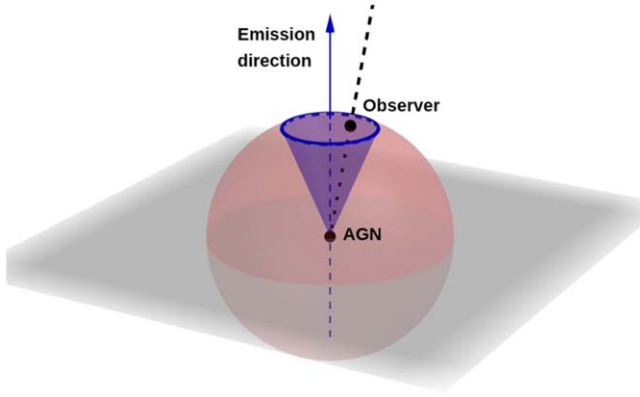


Figure 2. The emission from the blazar centered on the sphere is assumed to be constricted within the blue cone. The black dashed line represents the line of sight toward the center of the sphere for an observer on the surface.

$\theta \lesssim 1/\Gamma$. Now, the flux of secondary cascade photons will be distributed across the area of the spherical cap subtended on the surface of the sphere by the emission cone.

DINT solves the transport equation in 1D for the propagation and electromagnetic cascade of secondary e^+ , e^- , and γ photons produced from UHECR interactions with the CMB and EBL. Hence, we run 1D simulations in CRPropa for the propagation of UHECRs, producing EM particles, to calculate the secondary photon flux at the Earth. To find the flux intercepted by the observer's line of sight in the presence of an EGMF, we multiply this photon flux by ξ_B . Although ξ_B is calculated for an observer sphere of radius $R_{\text{obs}} = 1$ Mpc, this introduces little error as $l_c = 1$ Mpc, and also the mean free path for energy loss of UHECRs in the energy range considered is much greater than this value (Dermer et al. 2009; Heiter et al. 2018). In this process, we already reject the contribution to secondary photons from all UHECRs outside of $0^\circ.1$ with respect to the propagation direction along which the observer is located.

Thus, the luminosity required in UHECR protons, L_{UHECR} can be calculated from the expression

$$L_{\text{UHECR}} = \frac{2\pi d_L^2 (1 - \cos \theta_{\text{jet}})}{\xi_B f_{\text{CR}}} \int_{\epsilon_{\gamma, \text{min}}}^{\epsilon_{\gamma, \text{max}}} \epsilon_{\gamma} \frac{dN}{d\epsilon_{\gamma} dAdt} d\epsilon_{\gamma} \quad (15)$$

where $2\pi d_L^2 (1 - \cos \theta_{\text{jet}})$ is the area of the spherical cap region. We consider typical values of $\theta_{\text{jet}} \sim 0.1$ radians (Pushkarev et al. 2009; Finke 2019). f_{CR} is the ratio of the power in produced secondary photons $L_{\gamma, p}$ due to propagation of UHECRs and cascade of resulting EM particles, to the injected UHECR power L_{UHECR} . Both ξ_B and f_{CR} will be a function of propagation distance. The values of these quantities obtained for the sources in our study, while modeling the VHE γ -ray component, are listed in Table 1. The integral is over the flux of secondary photons of hadronic origin, required to fit the observed blazar SED. We obtain the secondary EM particles and cascade photons from 1D simulations, and account for the conical distribution by calculating the luminosity according to Equation (15).

The observed photon flux from inside the jet will be attenuated due to absorption in the EBL and is taken into account using the Gilmore et al. model. The optical depth for a gamma-ray observed at energy E_{γ} is calculated by the following integral along the line of sight to the target at

Table 1
UHECR Model Parameters

HBL	z	d_L	ξ_B	f_{CR}	f_{ν}
1ES 1011+496	0.212	1085 Mpc	0.45	0.084	0.00064
1ES 0229+200	0.140	687 Mpc	0.46	0.052	0.00039
1ES 1101-232	0.186	938 Mpc	0.48	0.079	0.00058
1ES 0414+009	0.287	1529 Mpc	0.39	0.085	0.00077

redshift z (Gilmore et al. 2012),

$$\tau(E_{\gamma}, z_0) = \frac{1}{2} \int_0^{z_0} dz \frac{dl}{dz} \int_{-1}^{+1} du (1 - u) \times \int_{E_{\text{min}}}^{\infty} dE_{\text{bg}} n(E_{\text{bg}}, z) \sigma(E_{\gamma}(1+z), E_{\text{bg}}, \theta) \quad (16)$$

where E_{min} is the redshifted threshold energy E_{th} for a background photon to interact with a γ -ray of energy E_{γ} .

$$E_{\text{min}} = E_{\text{th}}(1+z)^{-1} = \frac{2m_e^2 c^4}{E_{\gamma}(1+z)(1-\cos\theta)} \quad (17)$$

$n(E_{\text{bg}}, z)$ is the proper density of target background photons as a function of energy E_{bg} and redshift z , and $u = \cos\theta$. dl/dz is the cosmological line element given by

$$\frac{dl}{dz} = \frac{c}{(1+z)H_0} \frac{1}{\sqrt{\Omega_m(1+z)^3 + \Omega_{\Lambda}}}. \quad (18)$$

The attenuation affects only the high-energy end of the SSC spectrum, as can be seen in Figure 4 producing a flux $F_{\gamma}^{\text{obs}}(E, z) = F_{\gamma}^{\text{int}}(E, z) \exp[-\tau(E_{\gamma}, z_0)]$. An intuitive treatment of $\gamma\gamma_{\text{bg}}$ attenuation is also done in Razzaque et al. (2009; see their Equation (17)). The attenuation effect on the cascade photons due to the EBL is incorporated in the DINT code. We implement the Gilmore et al. EBL model in the DINT for propagation and cascade initiated by secondary EM particles. Our results do not depend significantly on the choice of other recent EBL models, e.g., Finke et al. (2010) and Domínguez et al. (2011).

We consider the sources: 1ES 1011+496, 1ES 0229+200, 1ES 1101-232, and 1ES 0414+009. These representative class of HBLs covers a wide range in redshift (indicated in Table 1) and hence provides a laboratory for testing the plausibility of γ -ray production from UHECR interactions. First, we calculate the timescale of photopion and Bethe-Heitler interactions $t_{p\gamma}$, t_{BH} , inside the jet and compare it with the escape timescale t_{esc} , using Equations (7) and (9). The seed photons are considered to be synchrotron as well as IC photons. We also calculate the acceleration timescale t_{acc} using Equation (10). The various timescales and interaction rates are shown in Figure 3. In the Bohm diffusion approximation, the diffusion coefficient can be written as $D = \eta r_{Lc}/3$. However, particles can be more diffusive than this and we consider the Kraichnan model of diffusion with the diffusion coefficient D_0 adjusted between 10^{27} and 10^{30} $\text{cm}^2 \text{s}^{-1}$, such that the acceleration rate dominates over escape rate at least up to $E = 10^{19}$ eV. The maximum acceleration energy of protons inside the blob is found to be a few EeV from Equation (5), for the sources studied. In view of the dominance of acceleration over escape and uncertainties in fit parameters, we set $E_{p, \text{max}} = 10^{19}$ eV for all the sources

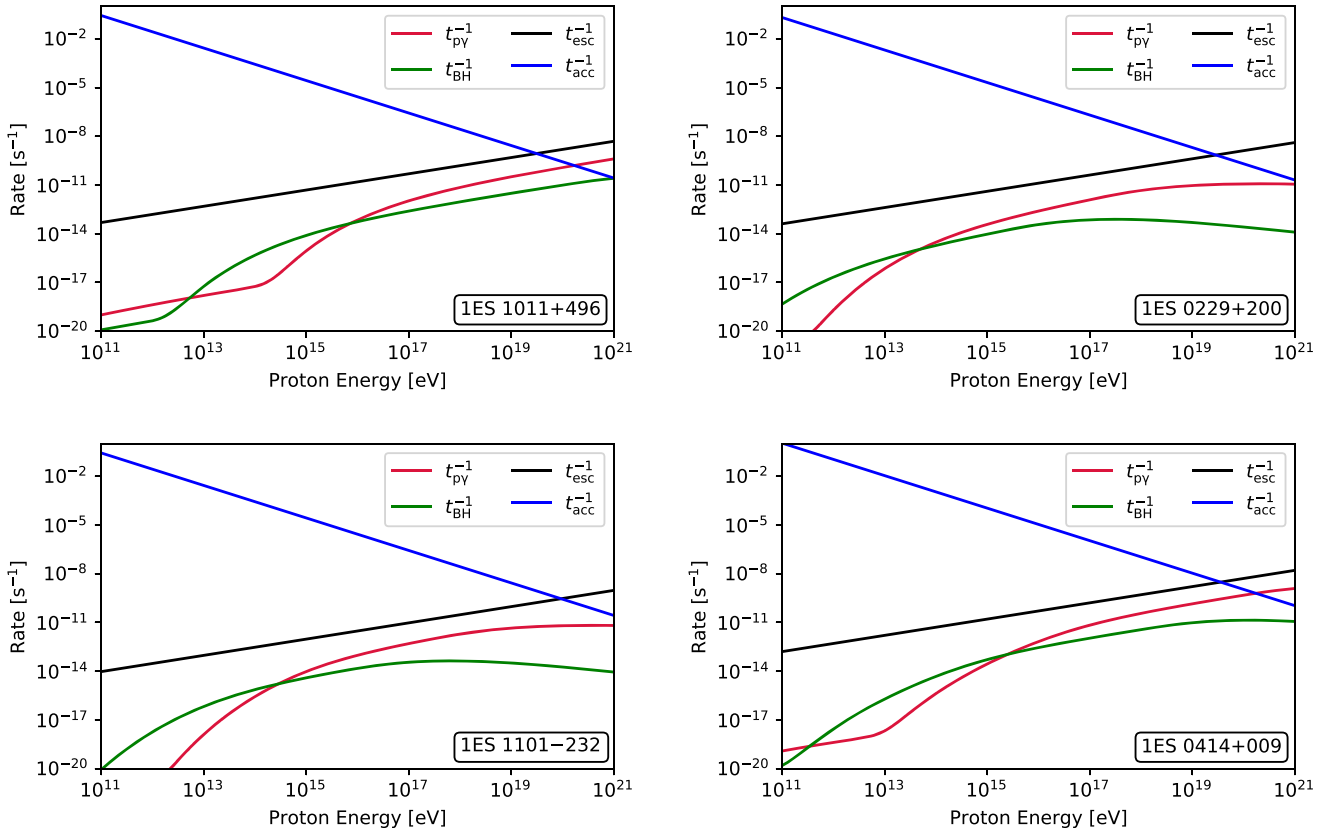


Figure 3. Timescale of photohadronic interactions inside the jet, with target photons from synchrotron and IC emission, calculated using Equation (7). The acceleration timescale (t_{acc}) and escape timescale (t_{esc}) are also shown for comparison, calculated from Equation (9) and (10), respectively. The Bohm condition gives the minimum diffusion, leading to a lower value of t_{esc} . Particles can be more diffusive than this, and thus t_{esc} is adjusted by varying the diffusion coefficient D_0 such that acceleration dominates up to 10^{19} eV (see text for more details). The $p\gamma$ and Bethe–Heitler interaction rates are found to be orders of magnitude less than the escape rate. The photon spectrum from π^0 decay inside the jet is calculated and found to be ~ 10 orders of magnitude less than the peak VHE flux, for the same normalization as required for contribution from UHECR interactions.

considered. The Eddington luminosity of the blazars can be calculated using the expression $L_{\text{Edd}} = 10^{47}(M_{\text{BH}}/10^9 M_{\odot}) \text{ erg s}^{-1}$. In the absence of an estimated BH mass, we consider $M_{\text{BH}} = 10^9 M_{\odot}$ for 1ES 1101–232. For the other sources, the masses of the SMBHs are taken from Falomo et al. (2003). We assume $\delta_D \simeq \Gamma$ in our calculations, which is valid for a viewing angle of the order of few degrees.

The synchrotron spectrum is modeled using a one-zone leptonic emission in GAMERA. The jet parameters obtained from the fit are used to calculate the SSC spectrum and adjusted to extend up to the highest energy possible. Beyond this energy, the hadronic contribution dominates. The photon spectrum produced in UHECR interactions, peaking at $\sim \text{TeV}$ energies, is incorporated to well explain the data points in the entire VHE range. The synchrotron and SSC luminosities are Doppler boosted in the observer frame by δ^4 . Here the multiwavelength data is taken for the quiescent state. The fit to photon SEDs obtained from a pure-leptonic origin are presented in the left panels of Figure 4. The corresponding parameter values are given in the top section of Table 2. Petropoulou et al. (2015) have done a detailed analysis of hadronic losses inside the jet resulting in photon spectrum in the HE regime. The proton jet power is much higher in Petropoulou et al. (2015) compared to ours. We have calculated the efficiency of $p\gamma$ interactions inside the jet using the formalism in Kelner & Aharonian (2008) and found that the photon spectrum resulting from π^0 decay is insignificant in comparison to the observed flux. Thus, we consider only the

interactions of UHECR protons during propagation over cosmological distances. The SSC flux depends on the radius of the spherical blob of emitting zone inside the jet and is adjusted suitably in case of a lepto-hadronic fit. The fit parameters used to model the observed SEDs using a combined leptonic + hadronic (UHECR) scenario are listed in the bottom section of Table 2 and the multiwavelength fits are presented in the right panels of Figure 4.

1ES 1011+496. The optical data, X-ray data, and radio-to-X-ray flux ratio show typical properties of an HBL (Padovani & Giommi 1995; Ahnen et al. 2016). It is situated at a redshift $z = 0.212$ and the VHE γ -ray emission was first discovered by MAGIC observations triggered by an optical outburst in March 2007 (Albert et al. 2007). The source has been well observed in the 0.1–300 GeV band by *Fermi*-LAT (Fermi-LAT Collaboration et al. 2015) and 0.3–10 keV band by *Swift*-XRT (Abdo et al. 2010). The source is also listed in the second catalog of hard *Fermi*-LAT sources. A photohadronic scenario to explain the HE SED is employed in Sahu et al. (2017). The flux value of the low-energy and HE peak are comparable. We find that the pure-leptonic model is unable to cover the highest-energy data points due to EBL attenuation. Increasing $E_{e,\text{cut}}$ worsens the fit for synchrotron spectrum. In the lepto-hadronic fit, photon spectrum from UHECR interactions can indeed explain the highest-energy data points.

1ES 0229+200. This BL Lac object at redshift 0.140 (Woo et al. 2005) shows an extremely hard intrinsic TeV spectrum with the synchrotron spectrum peaking at exceptionally high

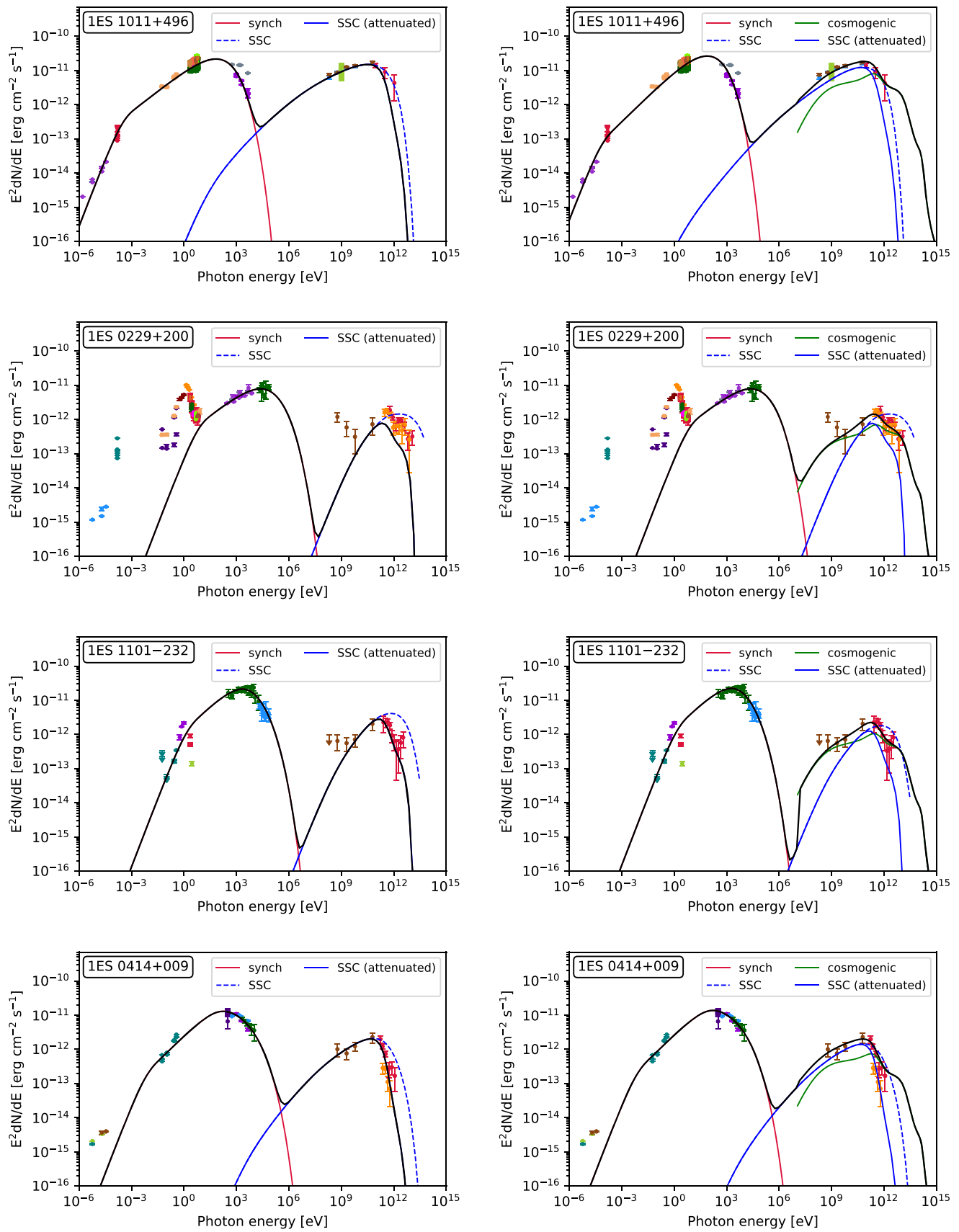


Figure 4. Multiwavelength spectrum of the HBLs, modeled using a pure-leptonic model (left) and a leptonic + hadronic model (right).

Table 2
Fit Parameters for the Multiwavelength SED Modeling in Figure 4

HBL	$E_{e,\min}$ (GeV)	$E_{e,\text{cut}}$ (GeV)	α	R (cm)	B (Gauss)	δ_D	L_e (erg s ⁻¹)	L_B (erg s ⁻¹)	L_{UHECR} (erg s ⁻¹)	L_{Edd} (erg s ⁻¹)
Pure-leptonic model										
IES 1011+496	0.08	75.0	2.2	1.5×10^{17}	0.024	20	5.8×10^{38}	1.9×10^{43}
IES 0229+200	10.00	1500.0	2.2	1.0×10^{16}	0.015	40	1.3×10^{38}	1.3×10^{41}
IES 1101-232	5.70	550.0	2.0	8.4×10^{16}	0.020	22	6.0×10^{37}	5.1×10^{42}
IES 0414+009	0.20	200.0	2.0	7.0×10^{16}	0.080	22	7.6×10^{37}	5.7×10^{43}
Leptonic + hadronic (UHECR) model										
IES 1011+496	0.04	65.0	2.0	2.2×10^{17}	0.020	20	3.8×10^{38}	2.9×10^{43}	4.8×10^{44}	5.1×10^{46}
IES 0229+200	10.00	1500.0	2.2	1.0×10^{16}	0.015	40	1.3×10^{38}	1.3×10^{41}	2.6×10^{43}	1.7×10^{47}
IES 1101-232	5.70	500.0	2.0	1.4×10^{17}	0.020	22	3.5×10^{37}	1.4×10^{43}	3.0×10^{43}	1.0×10^{47}
IES 0414+009	0.20	200.0	2.0	9.0×10^{16}	0.080	22	5.9×10^{37}	9.4×10^{43}	1.0×10^{44}	2.0×10^{47}

energies near the hard X-ray regime (Costamante et al. 2018). It has one of the highest IC peak frequency and the narrowest electron distribution among the extreme blazars known (Kaufmann et al. 2011). The source was first discovered by HESS in 2004 (Aharonian et al. 2007a). The X-ray-to-radio flux ratio classifies it as an HBL (Giommi et al. 1995). The SED in the HE band has been modeled using reprocessed GeV emission from pair production in the EBL and subsequent cascade (Tavecchio et al. 2010), using a similar method applied to γ -ray bursts in Razaque et al. (2004). The HE data is obtained from *Fermi*-LAT (Ackermann et al. 2013) and the VHE data is obtained from the HESS (H.E.S.S. Collaboration et al. 2014) and VERITAS collaborations (Cerruti 2013; Aliu et al. 2014). In our pure-leptonic modeling, there is no significant change in the SSC spectrum on increasing $E_{e,\text{cut}}$ beyond the value considered due to KN suppression. We show that the necessity of an additional component is inevitable and the spectrum arising from UHECR interactions well explains the highest-energy data points.

IES 1101-232. This HBL resides in an elliptical host galaxy at redshift $z = 0.186$. It was first detected by Ariel-5 X-ray satellite and was misidentified with the A1146 galaxy cluster at redshift $z = 0.139$ (Maccagni et al. 1978; McHardy et al. 1981). The optical and radio data led to the correct identification as a BL Lac object (Buckley et al. 1985; Remillard et al. 1989). The highest-energy data points exhibit very hard TeV spectra, which has been explained earlier using hadronic origin inside the jet emission region (Cerruti et al. 2015). The HE and VHE γ -ray data is obtained from *Fermi*-LAT and HESS observations (Aharonian et al. 2007b; H.E.S.S. Collaboration et al. 2014). It can be seen that that the highest-energy data points are not well covered by the SSC spectrum alone in a pure-leptonic fit. The fit improves considerably in the entire VHE range with the addition of the hadronic component originating in UHECRs.

IES 0414+009. The optical spectrum of this HBL at redshift $z = 0.287$ is described by the sum of the emission due to a standard elliptical galaxy and a relatively flat power law (Halpern et al. 1991). It was first detected by the *HEAO 1* satellite (Gursky et al. 1978) in the energy range 0.2 keV–10 MeV. It is one of the furthest VHE blazars with very hard TeV γ -ray spectrum and well-determined redshift. The SMBH at the center has a mass $2 \times 10^9 M_\odot$ (Falomo et al. 2003). The HE (100 MeV–100 GeV) data is obtained from *Fermi*-LAT and the source is listed in the *Fermi* 4FGL catalog.

The VHE ($E > 100$ GeV) γ -ray data is taken from observations by the HESS (H.E.S.S. Collaboration et al. 2012) and VERITAS (Aliu et al. 2012) collaborations. Despite the attenuation due to EBL background, a good fit to the observed SED is achieved using a pure-leptonic model alone. However, the fit to data points at the highest energy improves on adding the photon spectrum from UHECR interactions.

The broadband SED of the sources is plotted from the archival data as retrieved from ASDC SED builder (Stratta et al. 2011). The data points in the radio band are obtained from GBT (Gregory et al. 1996), CLASSCAT (Myers et al. 2003), NIEPPOCAT (Nieppola et al. 2007), NVSS (Condon et al. 1998), *Planck* (Planck Collaboration et al. 2014), and *WMAP* (Wright et al. 2009) observations. The *Wide-field Infrared Survey Explorer* catalog gives the flux values in infrared energies (Wright et al. 2010). The data for optical–UV wavebands are found from the UV and optical telescope (UVOT) of the *Swift* observatory (Giommi et al. 2012) and the *Galaxy Evolution Explorer* catalog (Bianchi et al. 2011). *BeppoSax* (Beckmann et al. 2002), *XMM-Newton* (Watson et al. 2009), and *Swift*-XRT (D’Elia et al. 2013) provides the soft X-ray data, while the hard X-ray data is obtained from *Swift*-BAT observations (Baumgartner et al. 2013).

Now, because the survival rate of UHECRs within $0^\circ.1$ of the propagation direction toward the observer is found to vary between 39% and 48% at a distance of 1 Mpc from the observer and the turbulent correlation length is taken to be $l_c = 1$ Mpc, UHECR events from the source should arrive at Earth. Although γ -rays travel mostly undeflected once produced, the Galactic magnetic field (GMF), being many orders of magnitude stronger than the EGMF, can deflect the UHECRs significantly. The deflection suffered by UHECRs in the GMF can be approximated as (Dermer & Menon 2009)

$$\theta_{\text{def,MW}} \approx \frac{0.9}{\sin b} \left(\frac{60 \text{ EeV}}{E/Z} \right) \left(\frac{B}{10^{-9} \text{ G}} \right) \left(\frac{h_{\text{disk}}}{1 \text{ kpc}} \right) \quad (19)$$

where b is the galactic latitude of the source and h_{disk} is the height of the Galactic disk. The GMF may create a strong shadowing effect on the true location of the sources (Fraija et al. 2018). This makes a direct estimation of the observed event rate difficult. The computational efficiency of forward propagation accounting for magnetic field effects over large distances with a point observer is very low in CRPROPA 3. We

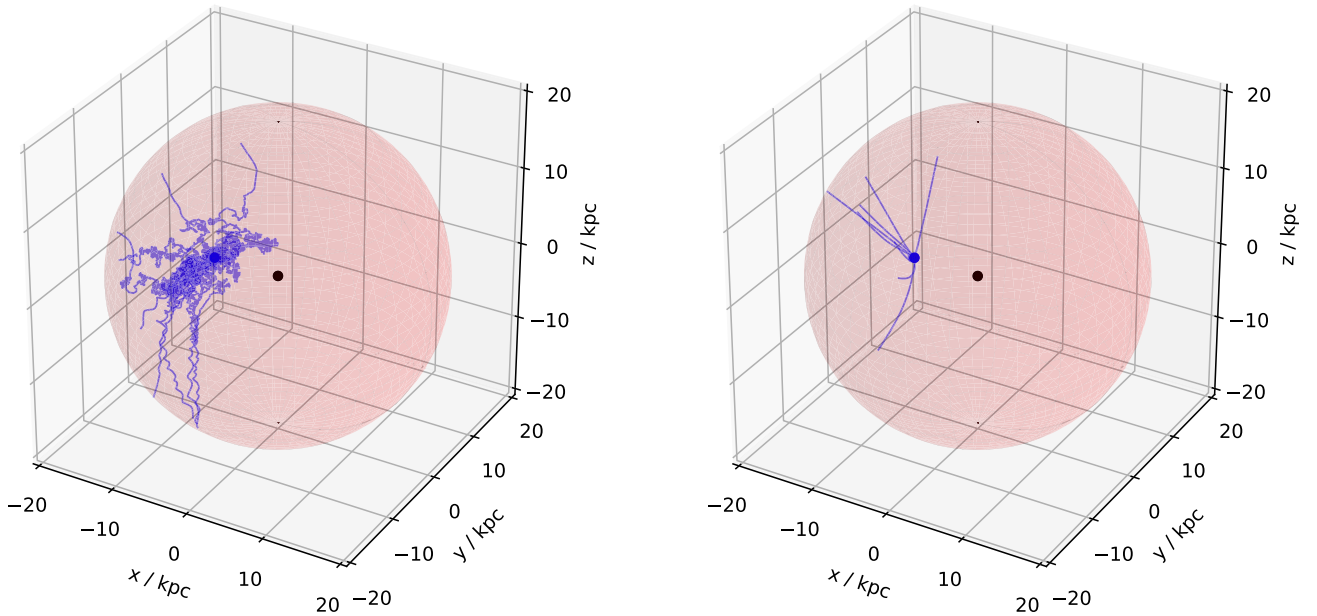


Figure 5. 3D trajectories of 10 UHECR anti-protons emitted isotropically and backtracked from the Earth in the Jansson & Farrar magnetic field of the Galaxy up to a halo radius of 20 kpc. The black dot indicates the Galactic center. See the text for more details. Left: for $E = 0.1$ EeV, the deflections are high and no directionality information can be retained. Right: for $E = 10$ EeV, the deflections are small and the anti-protons travel in almost straight lines, escaping the Galaxy.

do backtracking simulations of cosmic rays with opposite charge from the observer to the edge of the Galaxy for showing a graphical representation of UHECR trajectories in GMF. We consider a realistic magnetic field, such as that of Jansson & Farrar field model (JF12) with both random striated and random turbulent components (Jansson & Farrar 2012). For backtracking, 10 UHECR anti-protons are injected isotropically from the Earth and is similar to protons traveling toward Earth in forward simulations. In JF12 model the field is set to zero for $r > 20$ kpc and in a 1 kpc radius sphere centered on the Galactic center. The trajectories originating from Earth terminate at the boundary of the 20 kpc radius sphere. We consider two such cases when the UHECR protons are observed at Earth with $E_{\text{obs}} = 0.1$ and 10 EeV. The resulting trajectories are shown in the left and right panels of Figure 5, respectively. The black and blue dots represent the Galactic center and the Earth at a distance of 8.5 kpc from the Galactic center, respectively.

An estimate of the number of UHECR events that can be expected at the Pierre Auger observatory (PAO) in Malargüe, Argentina can be calculated from

$$N_{\text{evt},p} = \frac{1}{\xi_B} \frac{\Xi \omega(\delta)}{\Omega} \int_{E_{\text{th}}^{\text{obs}}}^{E_{\text{max}}^{\text{obs}}} \frac{dN}{dE} dE \quad (20)$$

where $\omega(\delta)$ is the relative exposure at a point source in the sky compared to the largest exposure on the sky (Somers 2001) and Ξ is the total integrated exposure over the detector's field of view. Here the additional factor ξ_B accounts for UHECRs surviving within $0^\circ.1$ of the initial propagation direction, at a distance of 1 Mpc from Earth. Since the maximum UHECR energy $E_{p,\text{max}}$ is taken to be only 10 EeV for all the sources, the UHECR events are subjected to large deflections in the GMF. The value of $E_{\text{th}}^{\text{obs}}$ being smaller compared to the GZK cutoff energy (Greisen 1966; Zatsepin & Kuzmin 1966), or the energy

threshold for AGN correlation analysis by PAO (Pierre Auger Collaboration et al. 2008), an intermediate-scale anisotropy study is difficult to do. Also in large-scale anisotropic studies, the most significant signal found is the dipolar modulation in R.A. at energies $E > 8$ EeV (Pierre Auger Collaboration et al. 2017, 2018). In the latter case, a statistically significant oversampling at any grid point in the sky, compared to background events, is unexpected owing to the deflection and huge number of observed events at these low energies. Therefore, if the energy of the UHECRs from the HBLs we considered is restricted to below 10 EeV as required by our model, then it will be difficult to detect them directly as discussed in Razzaque et al. (2012).

Since neutrinos travel unhindered by interactions and undeflected by magnetic fields, the neutrinos produced from the sources near to the line-of-sight direction are expected to arrive at Earth. The obtained luminosity in neutrinos is constrained from the luminosity requirement in UHECRs to explain the VHE γ -ray flux. Thus, we can write

$$L_\nu = L_{\text{UHECR}} \times f_{\text{CR} \rightarrow \nu} \times \xi_B \quad (21)$$

where $f_{\text{CR} \rightarrow \nu}$ is the ratio of the power in produced secondary neutrinos $L_{\nu,p}$ due to propagation of UHECRs, to the injected UHECR power L_{UHECR} . This gives the normalization of secondary neutrino flux arriving within $0^\circ.1$ of the direction of propagation in which the observer is situated. The resulting all-flavor neutrino fluxes are shown in Figure 6. The extrapolated three-year sensitivities for the proposed future detectors POEMMA (Adams et al. 2017; Olinto et al. 2017) and the 200,000 antenna array GRAND-200K (Fang et al. 2017; Martineau-Huynh et al. 2017) are also shown. The detector sensitivities are multiplied by 4π steradians to obtain the isotropic sensitivity that can be compared with the calculated neutrino flux in units of $\text{eV cm}^{-2} \text{s}^{-1}$. A three-year full operation by these detectors will not be sufficient to constrain the neutrino flux from the sources studied.

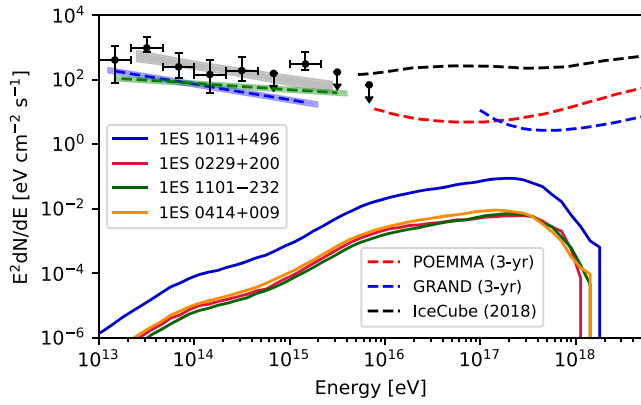


Figure 6. All-flavor neutrino flux at Earth produced in the same UHECR interactions as producing EM particles. The POEMMA and GRAND-200K sensitivities are multiplied by 4π steradians to compare with the neutrino fluxes in the same units. The differential upper limit on extremely high-energy cosmic neutrino flux by IceCube is also shown (Aartsen et al. 2018). The black data points show the observed astrophysical diffuse neutrino flux (Aartsen et al. 2015). The flux upper limit from 2LAC blazars is shown using equal weighting for a power law with spectral index 2.5 (blue-shaded region) and 2.2 (green-shaded region; Aartsen et al. 2017).

The secondary neutrino flux from 1ES 1011+496 is higher compared to the other sources. This is expected because of its higher flux value of the high-energy bump in the multi-wavelength SED, leading to a higher γ -ray flux required from hadronic interaction channels and hence a higher proton luminosity. The neutrino flux obtained peaks at 2.2×10^{17} eV. The IceCube eight-year differential flux upper limit (Aartsen et al. 2018), isotropized at this peak-energy, is of the order of 10^3 times higher than the peak flux from 1ES 1011+496, as shown in figure. Thus a possibility of detection of the neutrino flux obtained from the BL Lac objects in our study is unfavorable. The lower energy peak in the neutrino spectrum is not well pronounced because of the proton injection spectral index value $\alpha \sim 2$ considered for the sources. The observed astrophysical diffuse neutrino flux is shown in Figure 6. The gray-shaded region indicates the best-fit power law with spectral index ~ 2.5 (Aartsen et al. 2015). Assuming the neutrino flux follows the measured γ -ray energy flux exactly, the TeV–PeV upper limit from 2LAC blazars is also shown for two spectral indices, viz., 2.2 (shown in the green-shaded region) and 2.5 (shown in the blue-shaded region). This yields a maximum of 19%–27% contribution of the total 2LAC blazar sample to the observed best-fit value of the astrophysical neutrino flux (Aartsen et al. 2017).

4. Discussion

The one-zone leptonic emission model is often found to be inadequate in explaining the HE γ -ray spectrum of a number of BL Lac objects. These HBLs exhibit a hard intrinsic TeV spectrum, which requires an alternate explanation. In many studies, multi-zone emission is employed to fit the broadband spectrum up to the highest energies observed (see, e.g., Prince et al. 2019; Xue et al. 2019a). Among hadronic origin γ -ray models, those which invoke proton synchrotron emission requires extremely high kinetic power and very high values of Doppler factor or magnetic field (Petropoulou & Mastichiadis 2012). If protons are cooled efficiently by synchrotron photons produced from accelerated electrons, the contribution from photopion production, Bethe–Heitler interactions, and muon

synchrotron emission becomes important (Mannheim & Biermann 1992; Mücke et al. 2003).

In this study, we exploit yet another hadronic scenario where the UHECRs escaping from the jet can interact with cosmic background photons (CMB and EBL), to produce secondary electromagnetic particles. These particles can initiate EM cascades, during propagation over cosmological distances, leading to the production of the VHE γ -ray spectrum near the HE bump in the blazar SEDs (Essey & Kusenko 2010). Hadronic losses inside the blazar jet are found to be insignificant for the jet parameters considered in our model, facilitating the escape of UHECRs. For simplicity, we consider protons as the only UHECRs injected by these sources. We explain the multiwavelength SED of the HBLs by a suitable utilization of this lepto-hadronic model. The parameters for leptonic contribution is adjusted to extend the spectrum up to the highest energies possible and to simultaneously fit the synchrotron spectrum. Beyond this, the contribution from UHECR interactions dominate. The jet power required in such a scenario is calculated and compared with the Eddington luminosity.

We find that this model is successful in fitting the broadband emission spectrum of selected HBLs without exceeding the luminosity budget. The total proton luminosity L_p , considering relativistic protons down to ~ 10 GeV energies, will be approximately 5–10 times the L_{UHECR} value calculated. Taking this into account does not affect the credibility of our model, and the total jet power, in our case, still remains lower than L_{Edd} . It is shown in Razzaque et al. 2012, which required that L_{UHECR} increases with increasing values of the injection spectral index α and decreasing values of $E_{p,\text{min}}$. They have found that the lower limit on the jet power exceeds the Eddington luminosity for injection spectral index $\alpha > 2.2$ for all the sources considered. In our analysis, we restrict ourselves to $\alpha \leq 2.2$.

The value of ξ_B considered in the analysis is the survival rate of UHECRs within $0^\circ.1$ of the initial propagation direction. This is not the same as $0^\circ.1$ within the line of sight of the observer because the origin of angle is different in the two cases. Such a restriction provides increased constraints, which decreases the observed photon flux and thus increases the required UHECR power. The two has a one-to-one correspondence depending on the source distance. Hence, this factor is important to constrict the propagation within a narrow cone leading to an increased probability of interception by the observer. This is not considered in earlier works, thus reducing the luminosity requirement in UHECRs. If we calculate the survival rate of UHECRs within a smaller deflection angle than $0^\circ.1$, a lower value of EGMF will be necessary for a substantial contribution to photon flux from UHECR interactions. The value of B_{rms} considered in our study is 10^{-5} nG, which is higher than the lower limit estimated in Essey et al. (2011a).

Secondary charged EM particles produced within $0^\circ.1$ of the direction of propagation can still get deflected by the EGMF or GMF, reducing the observed cascade flux. This is not accounted for in the study. But it is also possible that contribution from shower development initiated outside of $0^\circ.1$ of the propagation direction is intercepted along the line of sight. But the energy-loss timescale of electrons/positrons being very low compared to protons, the fraction of events lost by such EM deflection should be negligible. Also, calculating ξ_B only up to 1 Mpc introduces very negligible error because

only an infinitesimal fraction of total EM particles are produced nearer to 1 Mpc from the Earth and the coherence length is set to $l_c = 1$ Mpc. We checked the fraction for 1ES 1011+496 at $d_c = 895$ Mpc from 1D simulation, accepting 100% of the produced events along the propagation direction. The fraction of EM events produced at distances less than 1 Mpc is found to be 0.0006.

Since the acceleration rate dominates over the escape rate up to $\gtrsim 10^{19}$ eV and the maximum energy obtained from the Hillas condition comes out to be a few EeV, we consider $E_{p,\max} = 10^{19}$ eV in our analysis. This also accounts for the uncertainty in fit parameters arising because electrons lose energy much faster than protons and as a result they are restricted to a smaller region, while protons can travel larger distances without significant energy loss. Thus, the confinement regions of electrons and protons are most likely different. This can result in slightly different blob radii as viewed by electrons and protons. $E_{p,\max}$ is less than the threshold of photopion production in the CMB, allowing the UHECR protons to travel cosmological distances and interact with EBL relatively close to Earth (Essey & Kusenko 2010). Hence, photopion interactions with EBL photons are dominant. Also, the proton injection is modeled to be a simple power law instead of an exponential cutoff power law. This makes no difference as the observed spectrum is not sensitive to the intrinsic source spectrum owing to the dominance of secondary photons from line-of-sight UHECR interactions (Essey et al. 2011a). However, the choice of the injection spectral index (α) does have significant impact on the secondary neutrino spectrum. The lower energy peak becomes more and more prominent with higher values of α (see, e.g., Das et al. 2019).

The total kinetic power in UHECRs required to explain the VHE spectrum also depends on the redshift of the sources. For higher values of z , the conversion of UHECR energy to γ -ray energy will be higher and the value of f_{CR} will be higher. This will decrease the value of L_{UHECR} . Again, with increasing z , the survival rate of UHECRs along the line of sight decreases. The HBLs selected for the study span a wide range in redshift and the value is highest for 1ES 0414+009 ($z = 0.287$). In this case also, the jet power required is less than that of a $10^9 M_{\odot}$ SMBH. It is predicted in Essey et al. (2011b) that a hard intrinsic TeV spectrum of distant blazars showing no or little attenuation can be attributed to the fact that the production of secondary γ -rays, occurring near to the observer compared to the source distance, dominates the observed γ -ray signal at the VHE regime. This justifies the competency of the UHECR interaction model, implemented in explaining the HE γ -ray spectrum from distant AGNs.

In modeling the multiwavelength spectrum of blazar SEDs, an equipartition of energy density between magnetic fields and radiating particles is assumed in many studies to reduce the number of free parameters. In our pure-leptonic analysis, the emission region is far from equipartition. The ratio u'_e/u'_B is very small in our case. The values of the magnetic field considered inside the jet is already low and decreasing them further to lower u'_B will result in a poor fit for the synchrotron spectrum. A departure from equipartition results in more luminosity requirement than minimum, as is also obtained in Zacharias & Wagner (2016). But this does not pose a theoretical difficulty as long as $L_{\text{jet}} \lesssim L_{\text{Edd}}$, which is true in our case. In lepto-hadronic fits, the VHE emission being dominated by the hadronic component, the values of $(u'_e + u'_p)/u'_B$ are near to equipartition. The range of values

obtained are between 16 and 200 and similar to that obtained for photohadronic interactions inside the jet in Cerruti et al. (2015). However, the energy density in electrons in the lepto-hadronic case is still low, resulting in low values of u'_e/u'_B . Lowering the magnetic field value further disallows the Hillas condition from achieving the required $E_{p,\max}$ value (see Basumallick & Gupta 2017, for a detailed discussion). In Petropoulou & Mastichiadis (2015), a departure from equipartition results from extremely high and dominant values of u'_p due to photohadronic interactions inside the jet.

The neutrino flux from individual BL Lac objects obtained in our analysis is too low to be detected by currently operating and upcoming future detectors. A stacked flux from all BL Lac objects with a similar UHECR production mechanism that we discussed could be interesting, however. The spectral shape is in accordance with that found in Essey et al. (2010). However, the neutrino flux they obtained for 1ES 0229+200 is many orders of magnitude higher than that obtained in our calculations. The reason for this is the low-luminosity requirement in UHECRs, as the VHE spectrum is modeled in our analysis using a comparable contribution from leptonic and hadronic counterparts at the peak. This hybrid contribution results in low L_{UHECR} for all the sources we have studied. The flux of secondary neutrinos is inversely proportional to redshift and the scaling is valid as long as the UHECR protons remain within the angular resolution of the detector (Essey et al. 2011b). Such a pattern is not seen in our results because of different peak VHE γ -ray flux of the sources, resulting in different UHECR luminosity requirements and hence distinct values of L_p . Given the low maximum proton energy (10 EeV) required in our model, and deflections in the EGMF and GMF, identifying UHECRs coming from individual BL Lac objects we discussed will be difficult.

5. Conclusions

The hard intrinsic TeV spectrum of HBLs showing very little attenuation is an intriguing mystery in astroparticle physics. A fit to the multiwavelength SEDs of selected HBLs, over a wide redshift range, is obtained by invoking contributions from hadronic channels arising in UHECR interactions on cosmic background photons. The resulting lepto-hadronic spectrum is well equipped to explain the observed SED in the VHE regime, even for the sources at the highest redshift considered. AGN are extremely energetic astrophysical objects that can produce both γ -rays and UHECRs. However, energies beyond 10 EeV are not easily produced inside the jet. Thus, UHECR interactions with the EBL dominate during cosmological propagation. For a substantial contribution from UHECR interactions, the protons must be collimated along the line of sight of the observer. The secondary particles produced from interactions of UHECRs with the EBL photons initiate EM cascades. With detailed modeling of these cascades and their propagation, we have shown that these contributions from UHECRs can fit VHE gamma-ray data beyond the applicability of the leptonic emission from the jets of a number of BL Lac objects.

The work of S.R. was partially supported by the National Research Foundation (South Africa) with grant No. 111749 (CPRR) and by the University of Johannesburg Research Council grant.

Software: CRPROPA 3 (Alves Batista et al. 2016), DINT (Lee 1998; Heiter et al. 2018), GAMERA (http://libgamera.github.io/GAMERA/docs/main_page.html).

Appendix

Effects of Maximum UHECR Energy $E_{p,\max}$

The spectrum of the observed γ -rays is governed primarily by the EM cascade of secondary particles produced from UHECR interactions with the CMB and EBL. The intrinsic source parameters have little or no effect on the VHE spectrum. However, the luminosity requirements can vary widely with source parameters, particularly $E_{p,\max}$, provided the UHECRs propagate for distances long enough to traverse multiple mean interaction lengths. In our work, we consider $E_{p,\max} = 10$ EeV based on the Hillas criterion and the comparison between acceleration and escape timescales (see Figure 3). But a different value obtained from different modeling can have a significant effect on L_{UHECR} due to increased or decreased interactions in the CMB and EBL. We check the effects due to the choice of maximum proton energy $E_{p,\max}$ on luminosity requirements. For this, we consider two values, $E_{p,\max} = 1$ and 100 EeV and fit the HE peak of the HBL 1ES 0414+009. This source has the highest redshift among those studied here. As a result, the effect of $E_{p,\max}$ variation on the survival rate of UHECRs along the line of sight, after suffering deflections in the EGMF, is expected to be the most prominent. The value of ξ_B is found to be 0.259 and 0.397 for $E_{p,\max}$ values of 1 and 100 EeV, respectively. The UHECR injection index is taken to be $\alpha = 2$, and all other parameters are kept the same as in Section 3. The ratio of power in produced γ -photons to the

injected UHECR power, f_{CR} is also calculated. The value of f_{CR} comes out to be 0.0052 and 0.2559, differing by two orders of magnitude, for $E_{p,\max}$ values 1 and 100 EeV respectively. The resultant fits are shown in the left and middle panels of Figure 7. The differences are negligible. The lower-energy part of the spectrum remains unchanged and hence is not shown.

The required luminosity is also found to differ by two orders of magnitude, being $2.47 \times 10^{45} \text{ erg s}^{-1}$ for $E_{p,\max} = 1$ EeV and $3.05 \times 10^{43} \text{ erg s}^{-1}$ for $E_{p,\max} = 100$ EeV. The distribution of EM particles produced from UHECR interactions at distance steps of 1 Mpc from the observer to the source is shown in Figure 8. For higher $E_{p,\max}$, more secondaries will be produced near the sources, tending to reduce the observed γ -rays along the line of sight. But the value of f_{CR} also increases for higher $E_{p,\max}$, due to increased photopion production on CMB, resulting in π^0 decay photons, and thus reducing the required value of L_{UHECR} , while for lower $E_{p,\max}$ the main contribution to the observed γ -ray signals comes from the EM cascade of e^+e^- pairs produced in Bethe–Heitler interactions with the CMB and EBL. Thus the relative dominance of various processes changes due to varying maximum energy. This also leaves an imprint on the subsequent neutrino spectrum. Resonant photopion production in the CMB with UHECRs of energy ~ 50 EeV produces the so-called GZK neutrinos and shifts the peak flux at higher energy. This can be seen in the right panel of Figure 7.

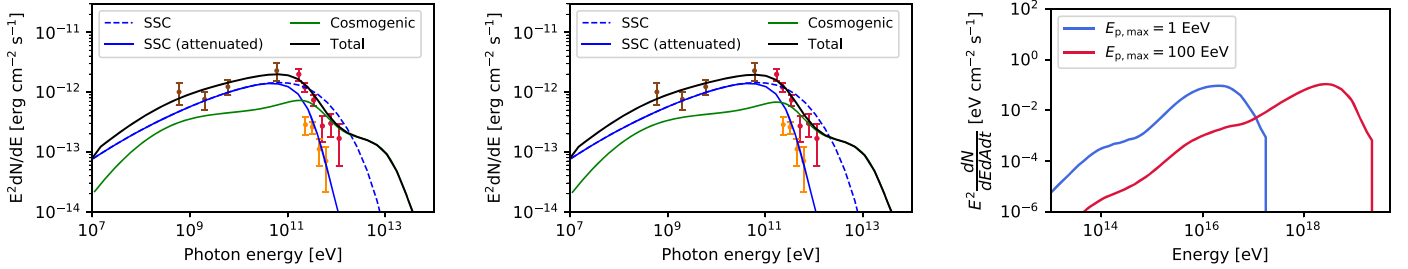


Figure 7. High-energy spectrum of the HBL 1ES 0414+009, fitted with varying maximum proton energy at the source. The left and middle panels show the fit for $E_{p,\max} = 1$ and 100 EeV, respectively. Not much variation can be seen in the spectral features. However, due to different survival rates in the EGMF and different energy conversion efficiency from UHECRs to γ -rays and neutrinos, the luminosity requirement at the source is different. The right panel shows the neutrino fluxes for both cases. See the main text for details.

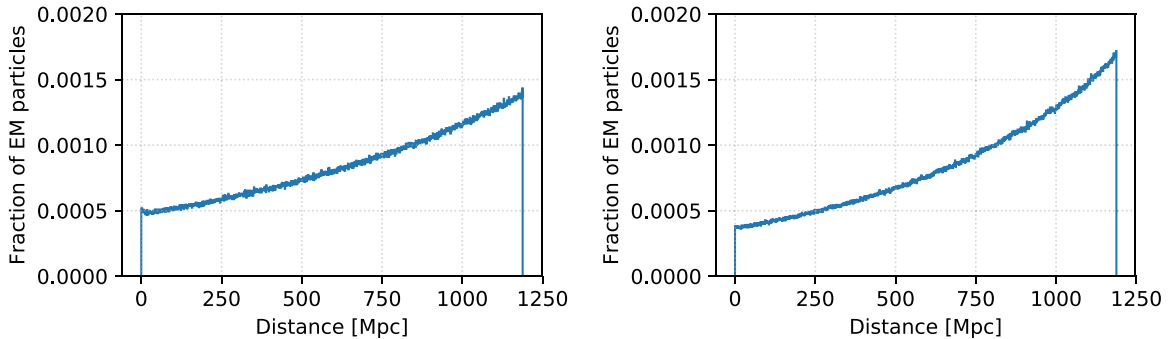


Figure 8. Fraction of total EM particles (e^+ , e^- , γ) produced from UHECR interactions, binned over distance from the observer, for proton energy cutoff $E_{p,\max} = 1$ EeV (left) and 100 EeV (right). The source is at $d_c \sim 1189$ Mpc.

ORCID iDs

Saikat Das  <https://orcid.org/0000-0001-5796-225X>
 Nayantara Gupta  <https://orcid.org/0000-0002-1188-7503>
 Soebur Razzaque  <https://orcid.org/0000-0002-0130-2460>

References

- Aab, A., Abreu, P., Aglietta, M., et al. 2015, *PhRvD*, **91**, 092008
 Aartsen, M. G., Abraham, K., Ackermann, M., et al. 2015, *ApJ*, **809**, 98
 Aartsen, M. G., Abraham, K., Ackermann, M., et al. 2017, *ApJ*, **835**, 45
 Aartsen, M. G., Ackermann, M., Adams, J., et al. 2018, *PhRvD*, **98**, 062003
 Abdo, A. A., Ackermann, M., Agudo, I., et al. 2010, *ApJ*, **716**, 30
 Abeyssekara, A. U., Albert, A., Alfaro, R., et al. 2017b, *ApJ*, **843**, 40
 Abeyssekara, A. U., Alfaro, R., Alvarez, C., et al. 2017a, *ApJ*, **843**, 116
 Acciari, V. A., Ansoldi, S., Antonelli, L. A., et al. 2019, *MNRAS*, **486**, 4233
 Ackermann, M., Ajello, M., Allafort, A., et al. 2013, *ApJ*, **765**, 54
 Ackermann, M., Ajello, M., Atwood, W. B., et al. 2015, *ApJ*, **810**, 14
 Adams, J., Anchordoqui, L. A., Apple, J. A., et al. 2017, arXiv:1703.04513
 Aharonian, F., Akhperjanian, A. G., Barres de Almeida, U., et al. 2007a, *A&A*, **475**, L9
 Aharonian, F., Akhperjanian, A. G., Bazer-Bachi, A. R., et al. 2006, *Natur*, **440**, 1018
 Aharonian, F., Akhperjanian, A. G., Bazer-Bachi, A. R., et al. 2007b, *A&A*, **470**, 475
 Aharonian, F. A. 2002, *MNRAS*, **332**, 215
 Ahnen, M. L., Ansoldi, S., Antonelli, L. A., et al. 2016, *MNRAS*, **459**, 2286
 Albert, J., Aliu, E., Anderhub, H., et al. 2007, *ApJL*, **667**, L21
 Aliu, E., Archambault, S., Arlen, T., et al. 2012, *ApJ*, **755**, 118
 Aliu, E., Archambault, S., Arlen, T., et al. 2014, *ApJ*, **782**, 13
 Alves Batista, R., Dundovic, A., Erdmann, M., et al. 2016, *JCAP*, **2016**, 038
 Basumallick, P. P., & Gupta, N. 2017, *ApJ*, **844**, 58
 Baumgartner, W. H., Tueller, J., Markwardt, C. B., et al. 2013, *ApJS*, **207**, 19
 Beckmann, V., Wolter, A., Celotti, A., et al. 2002, *A&A*, **383**, 410
 Berezinskii, V. S., & Grigor'eva, S. I. 1988, *A&A*, **199**, 1
 Berezinsky, V., Gazizov, A., & Grigorieva, S. 2006, *PhRvD*, **74**, 043005
 Bianchi, L., Efremova, B., Herald, J., et al. 2011, *MNRAS*, **411**, 2770
 Böttcher, M., & Els, P. 2016, *ApJ*, **821**, 102
 Böttcher, M., Reimer, A., Sweeney, K., & Prakash, A. 2013, *ApJ*, **768**, 54
 Buckley, D. A. H., Tuohy, I. R., & Remillard, R. A. 1985, *PASAu*, **6**, 147
 Celotti, A., & Ghisellini, G. 2008, *MNRAS*, **385**, 283
 Cerutti, M. 2013, Proc. ICRC, (Rio de Janeiro, Brazil), **1003**
 Cerutti, M., Zech, A., Boisson, C., & Inoue, S. 2015, *MNRAS*, **448**, 910
 Chodorowski, M. J., Zdziarski, A. A., & Sikora, M. 1992, *ApJ*, **400**, 181
 Condon, J. J., Cotton, W. D., Greisen, E. W., et al. 1998, *AJ*, **115**, 1693
 Costamante, L., Bonoli, G., Tavecchio, F., et al. 2018, *MNRAS*, **477**, 4257
 Das, S., Razzaque, S., & Gupta, N. 2019, *PhRvD*, **99**, 083015
 D'Elia, V., Perri, M., Puccetti, S., et al. 2013, *A&A*, **551**, A142
 Dermer, C. D., & Menon, G. 2009, High Energy Radiation from Black Holes: Gamma Rays, Cosmic Rays, and Neutrinos (Princeton, NJ: Princeton Univ. Press), <https://cds.cern.ch/record/1225453>
 Dermer, C. D., Razzaque, S., Finke, J. D., & Atayan, A. 2009, *NJPh*, **11**, 065016
 Domínguez, A., Primack, J. R., Rosario, D. J., et al. 2011, *MNRAS*, **410**, 2556
 Essey, W., Ando, S., & Kusenko, A. 2011a, *Aph*, **35**, 135
 Essey, W., Kalashev, O., Kusenko, A., & Beacom, J. F. 2011b, *ApJ*, **731**, 51
 Essey, W., Kalashev, O. E., Kusenko, A., & Beacom, J. F. 2010, *PhRvL*, **104**, 141102
 Essey, W., & Kusenko, A. 2010, *Aph*, **33**, 81
 Falomo, R., Carangelo, N., & Treves, A. 2003, *MNRAS*, **343**, 505
 Fang, K., Alvarez-Muniz, J., Alves Batista, R., et al. 2017, Proc. ICRC, (Bexco, Busan, Korea), 996, arXiv:1708.05128
 Fermi-LAT Collaboration, Acero, F., Ackermann, M., et al. 2015, *ApJS*, **218**, 23
 Finke, J. D. 2019, *ApJ*, **870**, 28
 Finke, J. D., Razzaque, S., & Dermer, C. D. 2010, *ApJ*, **712**, 238
 Fraija, N., Aguilar-Ruiz, E., Galván-Gómez, A., Marinelli, A., & de Diego, J. A. 2018, *MNRAS*, **481**, 4461
 Ghisellini, G., Padovani, P., Celotti, A., & Maraschi, L. 1993, *ApJ*, **407**, 65
 Gilmore, R. C., Somerville, R. S., Primack, J. R., & Domínguez, A. 2012, *MNRAS*, **422**, 3189
 Giommi, P., Ansari, S. G., & Micol, A. 1995, *A&AS*, **109**, 267
 Giommi, P., Polenta, G., Lähteenmäki, A., et al. 2012, *A&A*, **541**, A160
 Gregory, P. C., Scott, W. K., Douglas, K., & Condon, J. J. 1996, *ApJS*, **103**, 427
 Greisen, K. 1966, *PhRvL*, **16**, 748
 Gursky, H., Bradt, H., Doxsey, R., et al. 1978, *ApJ*, **223**, 973
 Halpern, J. P., Chen, V. S., Madejski, G. M., & Chanan, G. A. 1991, *AJ*, **101**, 818
 Heiter, C., Kuempel, D., Walz, D., & Erdmann, M. 2018, *Aph*, **102**, 39
 H.E.S.S. Collaboration, Abramowski, A., Acero, F., et al. 2012, *A&A*, **538**, A103
 H.E.S.S. Collaboration, Abramowski, A., Aharonian, F., et al. 2014, *A&A*, **562**, A145
 Hillas, A. M. 1984, *ARA&A*, **22**, 425
 Jansson, R., & Farrar, G. R. 2012, *ApJ*, **757**, 14
 Joshi, J. C., & Gupta, N. 2013, *PhRvD*, **87**, 023002
 Kalashev, O. E., Kusenko, A., & Essey, W. 2013, *PhRvL*, **111**, 041103
 Kaufmann, S., Wagner, S. J., Tibolla, O., & Hauser, M. 2011, *A&A*, **534**, A130
 Kelner, S. R., & Aharonian, F. A. 2008, *PhRvD*, **78**, 034013
 Khalikov, E. V., & Dzhatdoev, T. A. 2019, arXiv:1912.10570
 Lagage, P. O., & Cesarsky, C. J. 1983, *A&A*, **125**, 249
 Lee, S. 1998, *PhRvD*, **58**, 043004
 Maccagni, D., Tarengi, M., Cooke, B. A., et al. 1978, *A&A*, **62**, 127
 Mannheim, K., & Biermann, P. L. 1992, *A&A*, **253**, L21
 Martineau-Huyhn, O., Bustamante, M., Carvalho, W., et al. 2017, in EPJ Web of Conf. 135, 7th International Conference on Acoustic and Radio EeV Neutrino Detection Activities (ARENA 2016), ed. S. Buitink et al. (Groningen: EPJ), 02001
 McHardy, I. M., Lawrence, A., Pye, J. P., & Pounds, K. A. 1981, *MNRAS*, **197**, 893
 Mücke, A., Engel, R., Rachen, J. P., Protheroe, R. J., & Stanev, T. 2000, *CoPhC*, **124**, 290
 Mücke, A., Protheroe, R. J., Engel, R., Rachen, J. P., & Stanev, T. 2003, *Aph*, **18**, 593
 Murase, K., Dermer, C. D., Takami, H., & Migliori, G. 2012, *ApJ*, **749**, 63
 Murase, K., Oikonomou, F., & Petropoulou, M. 2018, *ApJ*, **865**, 124
 Myers, S. T., Jackson, N. J., Browne, I. W. A., et al. 2003, *MNRAS*, **341**, 1
 Neronov, A., & Vovk, I. 2010, *Sci*, **328**, 73
 Nieppola, E., Tornikoski, M., Lähteenmäki, A., et al. 2007, *AJ*, **133**, 1947
 Olinto, A. V., Adams, J. H., Aloisio, R., et al. 2017, Proc. ICRC, (Bexco, Busan, Korea), 542
 Padovani, P., & Giommi, P. 1995, *ApJ*, **444**, 567
 Petropoulou, M., Dimitrakoudis, S., Padovani, P., Mastichiadis, A., & Resconi, E. 2015, *MNRAS*, **448**, 2412
 Petropoulou, M., & Mastichiadis, A. 2012, *MNRAS*, **426**, 462
 Petropoulou, M., & Mastichiadis, A. 2015, *MNRAS*, **447**, 36
 Pierre Auger Collaboration, Aab, A., Abreu, P., et al. 2017, *Sci*, **357**, 1266
 Pierre Auger Collaboration, Aab, A., Abreu, P., et al. 2018, *ApJ*, **868**, 4
 Pierre Auger Collaboration, Abraham, J., Abreu, P., et al. 2008, *Aph*, **29**, 188
 Planck Collaboration, Ade, P. A. R., Aghanim, N., et al. 2014, *A&A*, **571**, A28
 Prince, R., Gupta, N., & Nalewajko, K. 2019, *ApJ*, **883**, 137
 Pushkarev, A. B., Kovalev, Y. Y., Lister, M. L., & Savolainen, T. 2009, *A&A*, **507**, L33
 Razzaque, S., Dermer, C. D., & Finke, J. D. 2009, *ApJ*, **697**, 483
 Razzaque, S., Dermer, C. D., & Finke, J. D. 2012, *ApJ*, **745**, 196
 Razzaque, S., Meszaros, P., & Zhang, B. 2004, *ApJ*, **613**, 1072
 Remillard, R. A., Tuohy, I. R., Brissenden, R. J. V., et al. 1989, *ApJ*, **345**, 140
 Sahu, S., de León, A. R., & Miranda, L. S. 2017, *EPJIC*, **77**, 741
 Sahu, S., López Fortín, C. E., & Nagataki, S. 2019, *ApJL*, **884**, L17
 Sahu, S., Zhang, B., & Fraija, N. 2012, *PhRvD*, **85**, 043012
 Settimo, M., & De Domenico, M. 2015, *Aph*, **62**, 92
 Sommers, P. 2001, *Aph*, **14**, 271
 Stecker, F. V. 1968, *PhRvL*, **21**, 1016
 Stratta, G., Capalbi, M., Giommi, P., et al. 2011, arXiv:1103.0749
 Sapanitsky, A. D., & de Souza, V. 2013, *JCAP*, **2013**, 023
 Takami, H., Murase, K., & Dermer, C. D. 2013, *ApJL*, **771**, L32
 Tavecchio, F. 2014, *MNRAS*, **438**, 3255
 Tavecchio, F., Ghisellini, G., Foschini, L., et al. 2010, *MNRAS: Letters*, **406**, L70
 The Fermi-LAT Collaboration 2019a, arXiv:1902.10045
 The Fermi-LAT Collaboration 2019b, arXiv:1905.10771
 VERITAS Collaboration, Archer, A., et al. 2018, *PhRvD*, **98**, 062004
 Watson, M. G., Schröder, A. C., Fyfe, D., et al. 2009, *A&A*, **493**, 339
 Woo, J.-H., Urry, C. M., van der Marel, R. P., Lira, P., & Maza, J. 2005, *ApJ*, **631**, 762
 Wright, E. L., Chen, X., Odegard, N., et al. 2009, *ApJS*, **180**, 283
 Wright, E. L., Eisenhardt, P. R. M., Mainzer, A. K., et al. 2010, *AJ*, **140**, 1868
 Xue, R., Liu, R.-Y., Petropoulou, M., et al. 2019a, *ApJ*, **886**, 23
 Xue, R., Liu, R.-Y., Wang, X.-Y., Yan, H., & Böttcher, M. 2019b, *ApJ*, **871**, 81
 Zacharias, M., & Wagner, S. J. 2016, *A&A*, **588**, A110
 Zatsepin, G. T., & Kuzmin, V. A. 1966, *JETPL*, **4**, 78
 Zdziarski, A. A., & Böttcher, M. 2015, *MNRAS*, **450**, L21